Numerical Simulations of the Elbe Flood Case: Sensitivity to Initial and Boundary Data

Günther Zängl[1], Gisela Hartjenstein[1], Günther Doms[2] †, Helmut Frank[2] and Ulrich Schättler[2]

[1] *Meteorologisches Institut der Universität München*
[2] *Deutscher Wetterdienst, Offenbach am Main, Germany*

Abstract

LM simulations have been conducted to examine the reasons for the unsatisfying performance of the operational forecasts for the Elbe flood case in August 2002. We investigated the impact of different initial and boundary conditions, of the cloud microphysical scheme, and of the model resolution. The most important factor turned out to be related to the initial and boundary data. Taking the initial conditions from ECMWF analyses rather than from the operational DWD analyses greatly improves the intensity and spatial structure of the rainfall field. On the other hand, it is comparatively unimportant whether the lateral boundary data are taken from the ECMWF forecast or from a GME forecast initialized with ECMWF analysis data, provided that the horizontal resolution of the GME is similar to that of the ECMWF model. Regarding the cloud microphysical scheme of the LM, it proved to be important to account for the horizontal advection of precipitation particles. Otherwise, the simulated rainfall maximum in the Erzgebirge region is located too far upstream. Refining the model resolution from 7 km to 2.8 km combined with deactivating the convection scheme degrades the model performance because only part of the parameterized (convective) rainfall occurring at 7 km resolution is captured explicitly at 2.8 km resolution.

1 Introduction

In August 2002, the Elbe river catchment area in eastern Germany and the Czech Republic was struck by the heaviest flooding event ever recorded. The largest fraction of the rainfall responsible for the flood fell on 12 and 13 August in connection with a cyclone following the so-called Vb path (van Bebber, 1891), moving from the Adriatic Sea via the eastern edge of the Alps towards Poland. Specifically, the heavy rainfall was caused by a partly occluded warm front on the western and north-western side of the cyclone, which remained essentially stationary over eastern Germany for more than a day although the low-pressure core moved slowly north-eastward. As shown by Ulbrich et al. (2003), the large-scale lifting in the frontal zone was particularly intense because converging surface isobars were combined with pronounced upper-level divergence. Moreover, orographic lifting over the northern slopes of the mountain ranges located in the frontal area led to pronounced local precipitation maxima. The primary one was registered in the eastern part of the Erzgebirge, a mountain range located at the German-Czech border (see Fig. 1). According to the available raingauge measurements, an area of about 25×25 km^2 encountered 36-hour rainfall accumulations in excess of 250 mm, and a peak value of 394 mm was measured at a village named Zinnwald-Georgenfeld near the crest line of the Erzgebirge.

Although the global weather forecasts for 12/13 August 2002 indicated a Vb cyclone track already six days in advance, the operational forecasts of the precipitation field were quite

poor. Even the regional-scale Lokal-Modell (LM) forecasts of the German Weather Service (DWD) greatly underestimated the rainfall amounts associated with the cyclone, combined with a mislocation of the rainfall maximum. For example, the LM forecast started at 12 UTC on 11 August placed the primary rainfall maximum ($\sim$ 225 mm) 130 km too far east, affecting the Riesengebirge rather than the Erzgebirge, whereas the secondary rainfall maximum in the Erzgebirge reached only 150 mm (DWD, 2002; see also Fig. 3a). For this rainfall distribution, the Oder river would have been affected by a more severe flooding than the Elbe. In the subsequent forecasts, the rainfall maximum gradually moved westward but still remained significantly east of the observed location. As a consequence, the severe weather warnings issued by the DWD on August 11 were far from indicating a catastrophic flood, predicting only 40–80 mm within 24 hours (DWD, 2002). In the morning of August 12, the rainfall warning was enhanced to 70–120 mm, which would imply a serious flood but is still far below the observed values.

Numerical simulations with the MM5 conducted by Zängl (2004, hereafter Z04) showed a much better agreement with observations although the peak precipitation amounts in the Erzgebirge were still underestimated. Moreover, tests with different model configurations indicated that the model's capability to reproduce the orographic rainfall intensification in the Erzgebirge depends significantly on the model resolution. However, the reasons for the bad performance of the operational forecasts remained unresolved because the simulations presented by Z04 differ in too many aspects from the operational forecasts. This issue will be investigated in the present study, where we use the LM in order to ensure comparability with the operational forecasts. The focus of our sensitivity tests is on the impact of the initial and boundary conditions, but we will also consider the effect of the cloud microphysical parameterization and of the model resolution. The remainder of this note is structured as follows. The setup of the simulations is described in Section 2, followed by a description of the observed precipitation field and the verification methods in Section 3. Section 4 presents the results of the experiments, and a set of conclusions is drawn in Section 5.

2 Setup of the experiments

The sensitivity study reported here was performed with LM version 3.12 (Steppeler et al., 2003) Unless mentioned otherwise, our simulations are based on the operational setup of the LM with a horizontal mesh size of 7 km and 325×325 grid points (Fig. 1). Part of the sensitivity tests are conducted with a mesh size of 2.8 km and 421×461 grid points, corresponding to the domain of the LMK that is planned to become operational (see dashed box in Fig. 1).

The model experiments discussed in section 4 start with the operational forecasts initialized at 12 UTC on August 11 and 00 UTC on August 12 (denoted as OP-1112 and OP-1200, respectively). The OP runs are initialized with the operational nudging-based LM analysis and use GME forecasts as lateral boundary conditions. The GME forecasts are performed with a horizontal mesh size of 60 km and are initialized with the optimal interpolation scheme operationally used for the GME. The LM cloud microphysics scheme does not include the ice phase and does not account for the horizontal advection of precipitation particles (as was operational in 2002). Convection is parameterized with the operational Tiedtke (1989) scheme.

To determine the impact of the LM nudging analysis scheme, the second series of experiments is initialized directly from the GME analysis without applying other changes to the model setup. This series is denoted as GME60-LM-ddhh (ddhh = initialization day and hour). In addition, a re-analysis performed with a more recent GME version that includes ice

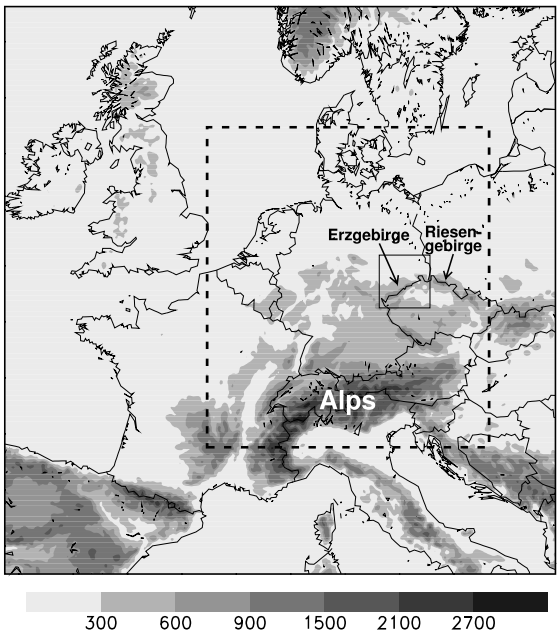

Figure 1: Model topography of the LM domain. The dashed and solid boxes indicate the LMK integration domain and the verification domain, respectively.

microphysics has been tested. For this series of tests, ice microphysics has also been used in the LM. In the simulation name, GME is replaced with GMI when the GME includes ice microphysics.

The remaining experiments are initialized with ECMWF analysis data. Since the ECMWF analyses include cloud ice, the ice phase is also accounted for in the LM microphysics scheme. For the lateral boundary conditions, three different configurations have been tested. The first one, denoted as EC-LM-ddhh, uses ECMWF forecasts corresponding to the respective analysis time. In the other configurations, the lateral boundary conditions are provided by a GME forecast (including ice) initialized with ECMWF analysis data. These GME forecasts have been conducted with a horizontal mesh size of either 60 km or 40 km, corresponding to the operational setup of 2002 and 2004, respectively. The latter series will be denoted as EC-GMIxx-LM-ddhh with xx indicating the GME grid size in km. These boundary data configurations are combined with two versions of the LM microphysics scheme, the more recent one of which accounts for the horizontal advection of precipitation particles. The latter scheme will be referred to as "prognostic precipitation" in the following, abbreviated as LMpp in the simulation acronyms. The sensitivity experiments conducted with the LMK configuration (2.8 km resolution) always include the prognostic precipitation scheme and thus are abbreviated as LMKpp. They differ from the coarser-resolved LM simulations in that the Tiedtke convection scheme is deactivated. However, the shallow convection scheme currently being developed for the LMK is not used because this scheme was not yet available at the time the simulations were conducted. Also, the dynamical core is the same as for the present LM. The LMK grid is one-way nested into the LM, implying that it receives the lateral boundary data from the corresponding LM forecast.

3 Observed precipitation field and verification methods

Since the synoptic evolution of the Elbe flood case is described in some detail in Ulbrich et al. (2003) and Z04, the observed precipitation field in the core precipitation area (see solid box in Fig. 1 for location) is only briefly discussed. Fig. 2 displays the 36-h accumulated

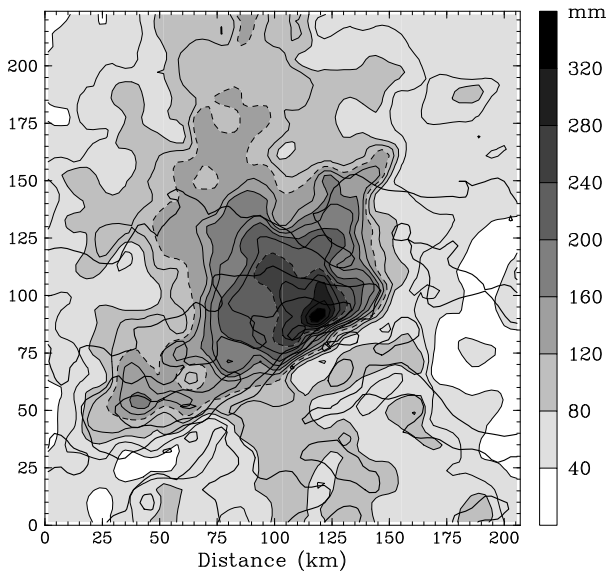

Figure 2: Observed accumulated precipitation (12 August 00 UTC – 13 August 12 UTC) interpolated on the LMK grid. Bold contours indicate the LMK topography (contour interval 200 m), thin contours and shading indicate precipitation at an increment of 20 mm and 40 mm, respectively. Contours for 120 mm and 240 mm are dashed.

precipitation (00 UTC 12 August – 12 UTC 13 August) in this area, roughly corresponding to 50–52°N, 12–15°E. The rainfall field has been constructed by interpolating the measurements from 530 raingauge stations to the LMK grid with a Gaussian weighting method (see Z04 for details). It reveals a wide precipitation band covering most of the verification domain, with precipitation accumulations ranging between 30 and 80 mm near the western and eastern edges and between 100 and 400 mm in the central part. Values exceeding 160 mm are restricted to the northern slope of the Erzgebirge range, indicating that orographic precipitation enhancement played an important role in this case. Analysis of radar data (not shown) reveals that significant precipitation started around 04 UTC on 12 August in the Erzgebirge region, implying that even the simulations started at 00 UTC had several hours to spin up the precipitation field.

The skill scores computed to validate the model results presented in the subsequent section against the precipitation data start with a bilinear interpolation of the simulated values to the locations of the 530 raingauges. This is appropriate in this case because the data density is close to the model resolution (Tustison et al., 2001). The interpolated model output data are then used to compute the relative bias (i.e. the bias normalized by the averaged observed precipitation), the canonical correlation coefficient, the root-mean-square error (rmse) and the mean absolute error (mae). The statistical error measures are summarized in Table 1.

In addition, we computed three standard skill scores based on contingency tables in order to show the dependence of the model performance on the precipitation amount. A contingency table counts the number of simulated and observed data points exceeding a certain threshold value ts, yielding four possible cases:

	$o_i \geq ts$	$o_i < ts$
$s_i \geq ts$	a	b
$s_i < ts$	c	d

Based on this contingency table, the bias score (BS), the false alarm rate (FAR) and the

Simulation	bias	corr	rmse	mae
OP-1112	−45%	0.29	71.7	58.9
OP-1200	−26%	0.22	65.5	48.3
GME60-LM-1112	−28%	−0.03	75.1	59.4
GME60-LM-1200	−18%	0.42	59.7	46.0
GMI60-LM-1112	−23%	0.40	58.6	44.2
GMI60-LM-1200	+6%	0.47	55.6	41.6
EC-LM-1112	−10%	0.65	45.4	32.6
EC-LM-1200	−1%	0.80	35.5	25.4
EC-GMI40-LM-1112	−14%	0.70	43.2	31.9
EC-GMI40-LM-1200	+5%	0.72	40.4	31.2
EC-GMI60-LM-1112	−21%	0.51	54.3	38.9
EC-GMI60-LM-1200	+14%	0.71	46.3	36.1
EC-LMpp-1112	−23%	0.74	43.6	31.8
EC-LMpp-1200	−13%	0.86	31.5	22.1
EC-GMI40-LMpp-1112	−29%	0.78	45.1	34.6
EC-GMI40-LMpp-1200	−12%	0.85	32.5	24.4
EC-GMI60-LMpp-1112	−36%	0.65	55.1	40.7
EC-GMI60-LMpp-1200	−4%	0.78	36.7	27.0
EC-LMKpp-1112	−32%	0.71	50.5	39.2
EC-LMKpp-1200	−23%	0.78	42.3	29.8

Table 1: Relative bias, canonical correlation coefficient (corr), root-mean-square error (rmse) and mean absolute error (mae) for all model experiments discussed in this paper.

equitable threat score (ETS) are defined as

$$\mathrm{BS} = \frac{a+b}{a+c}\,, \qquad \mathrm{FAR} = \frac{b}{a+b}\,, \qquad \mathrm{ETS} = \frac{a-h}{a+c+b-h}\,,$$

where $h = (a+b)(a+c)/(a+b+c+d)$. These quantities are displayed in Fig. 4 for ts ranging from 20 mm to 300 mm at steps of 10 mm.

4 Model results

The results of the operational forecasts OP-1112 and OP-1200 are shown in Fig. 3. Comparing the simulated fields with the observed one (Fig. 2) reveals that the forecasts not only underpredict the maximum precipitation amounts but also fail to capture the spatial structure of the precipitation field. OP-1112 exhibits a local precipitation maximum at approximately the right location, but the main precipitation field is located too far east, and the absolute rainfall maximum ($\sim$ 225 mm) is east of the verification domain in the north-western Riesengebirge (see DWD, 2002, and Hartjenstein et al., 2005). In the later operational forecast OP-1200, the primary rainfall maximum is closer to the observed location, but the overall pattern of the precipitation field differs even more from the observed one than for OP-1112. The statistical measures summarized in Table 1 corroborate that the predicted rainfall fields have a large negative bias and a bad spatial correlation with the observed field, the latter being even worse for OP-1200 than for OP-1112. The negative bias is also evident from the bias score displayed in Fig. 4a, being generally below 1 for the operational forecasts. Rainfall accumulations above 150 mm (OP-1112) and 210 mm (OP-1200) are completely missed, corresponding to a bias score of zero. Despite the large negative bias, both operational forecasts exhibit a substantial false alarm rate (FAR, Fig. 4b), reflecting the misplacement of the simulated rainfall maxima. To summarize, the operational forecasts exhibit effectively no skill, as indicated by an ETS fluctuating around zero (Fig. 4c).

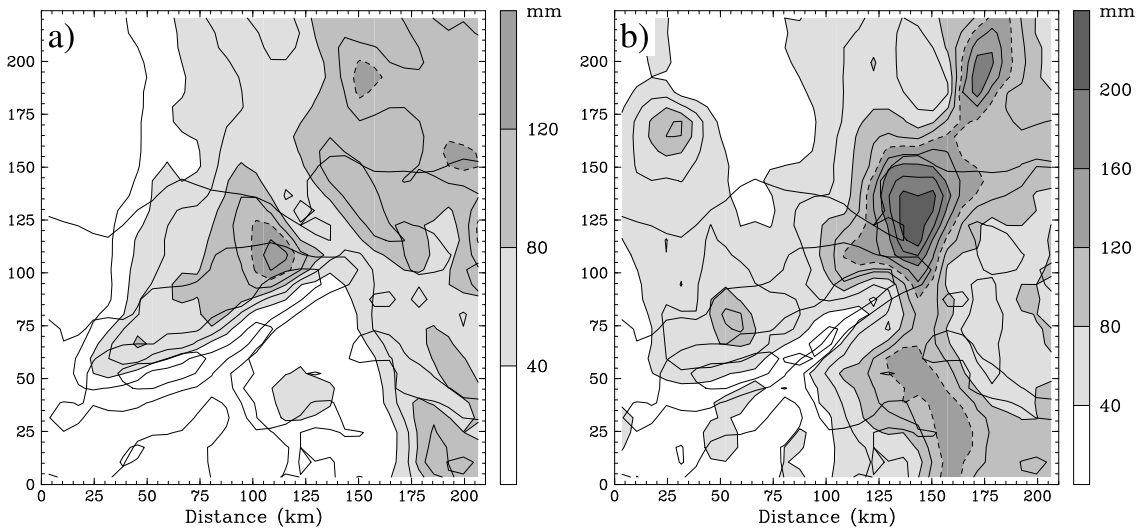

Figure 3: Simulated accumulated precipitation (12 August 00 UTC – 13 August 12 UTC) for experiments (a) OP-1112, (b) OP-1200. Plotting conventions are as in Fig. 2, but the model topography is shown for the LM.

Omitting the LM nudging analysis reduces the negative bias of the operational forecasts (Table 1 and Fig. 4a), but a slight improvement of the forecast quality is found only for the GME60-LM-1200 experiment. In the GME60-LM-1112 run, the mislocation of the precipitation field is even more pronounced than for OP-1112, yielding even larger error measures, a slightly negative correlation coefficient, a greatly increased FAR (Fig. 4b), and a negative ETS (Fig. 4c). Including ice-phase microphysics in the GME and the LM further increases the domain-averaged precipitation (Table 1, GMI60-LM series). Compared to the GME60-LM runs, the error measures indicate a notable improvement for 1112 but no clear tendency for 1200. In both cases, the spatial correlation between the simulated and observed precipitation fields is still unsatisfying.

Substantially better results are obtained when starting from ECMWF analysis data. As evident from Table 1, all the remaining experiments exhibit a higher correlation coefficient and lower error measures than the simulations initialized with the GME analysis. In addition, the lateral boundary data used during the forecast and the microphysical scheme (prognostic vs. diagnostic precipitation) play a significant role.

For the experiments with the diagnostic scheme (no horizontal advection of precipitation particles; 3rd section of Table 1), it can be seen that the forecasts started at 1200 perform better than those started at 1112. This behaviour is most pronounced for the EC-LM series that uses ECMWF forecasts as lateral boundary data. While the EC-LM-1112 run still exhibits a significant negative bias, EC-LM-1200 has almost no bias, and the other validation measures are also better for 1200 than for 1112. When taking the lateral boundary conditions from GME-forecasts based on ECMWF analyses, the negative bias increases for 1112 whereas a positive bias appears for 1200. Both effects also depend on the horizontal resolution of the GME, being larger at 60 km than at 40 km resolution. In addition, the verification results are generally worse for a GME resolution of 60 km than for 40 km. On the other hand, comparing the verification results for the EC-LM and EC-GMI40-LM series does not indicate a systematic signal.

Detailed verification results and accumulated precipitation fields are displayed in Figs. 4d–f and 5 for selected experiments. Fig. 5 readily shows that the spatial structure of the precipitation fields is closer to the observed one (Fig. 2) than for the operational forecasts (Fig. 3). In particular, the precipitation maximum is located in the right region, though being shifted

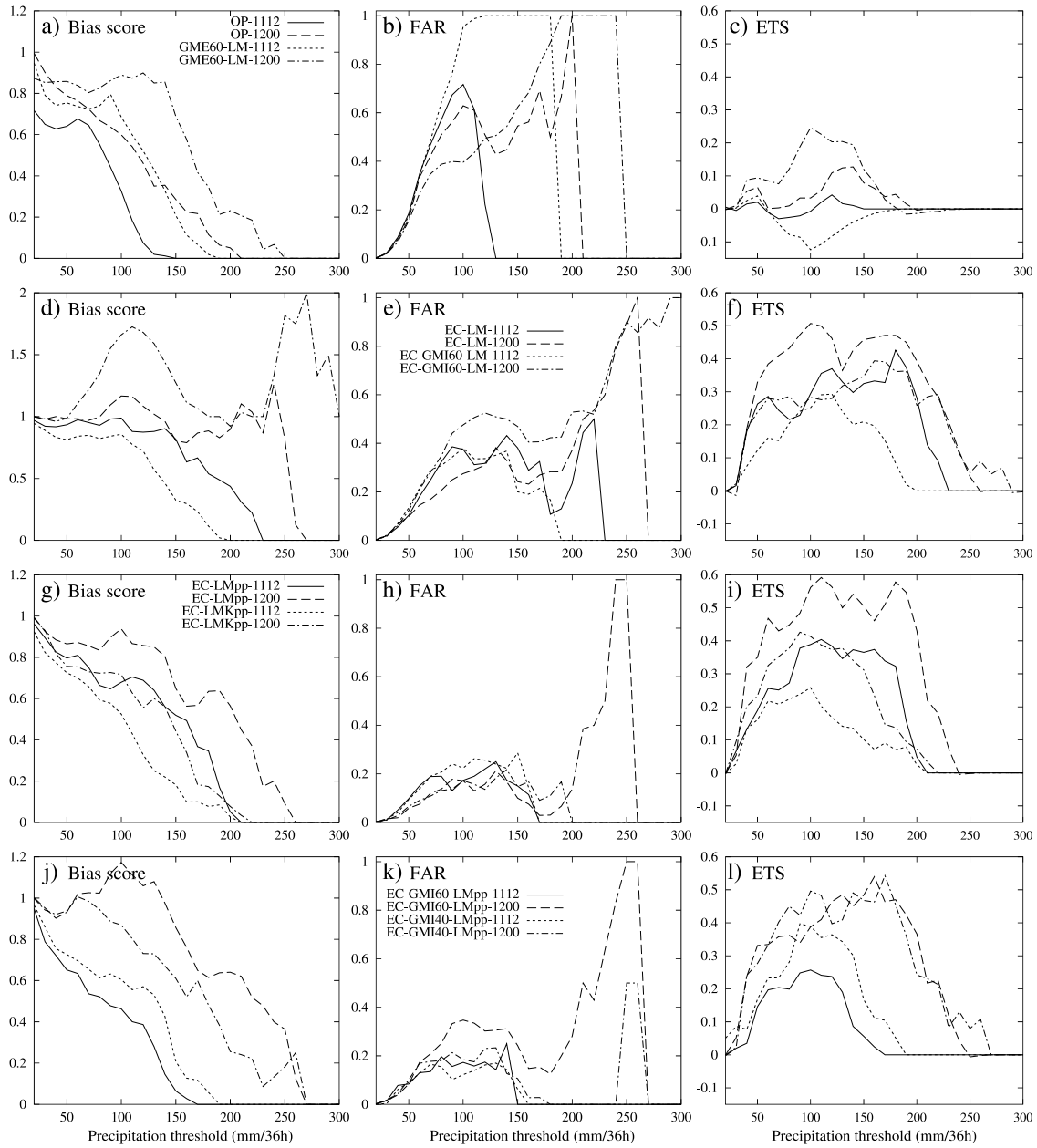

Figure 4: Bias score (left column), false alarm rate (FAR, middle column) and equitable threat score (ETS, right column) for various model experiments (see text for definition). The line keys given in (a), (e), (g) and (k) are valid for all panels of the respective row.

20–30 km upstream compared to the observations. Moreover, Fig. 5 confirms that the simulations started at 1200 produce higher precipitation amounts than those started at 1112. The bias scores shown in Fig. 4d indicate that EC-LM-1112 performs well at precipitation amounts below 150 mm but underestimates higher precipitation amounts, which is in accordance with the visual impression arising from Figs. 2 and 5a. An ETS of 0.3 up to a threshold of 200 mm (Fig. 4f) and a FAR below 0.4 (Fig. 4e) indicate that this forecast has significant skill. The ETS is even higher for the 36-h forecast (EC-LM-1200), combined with a bias score fluctuating around 1 up to a threshold of 250 mm. The high FAR at precipitation thresholds between 200 and 260 mm reflects the fact that the precipitation maximum is located incorrectly. Fig. 4d also shows that taking the lateral boundary conditions from a GME forecast performed at 60 km resolution (EC-GMI60-LM) increases the negative bias for 1112 whereas a substantial positive bias is created for the initialization at 1200. The

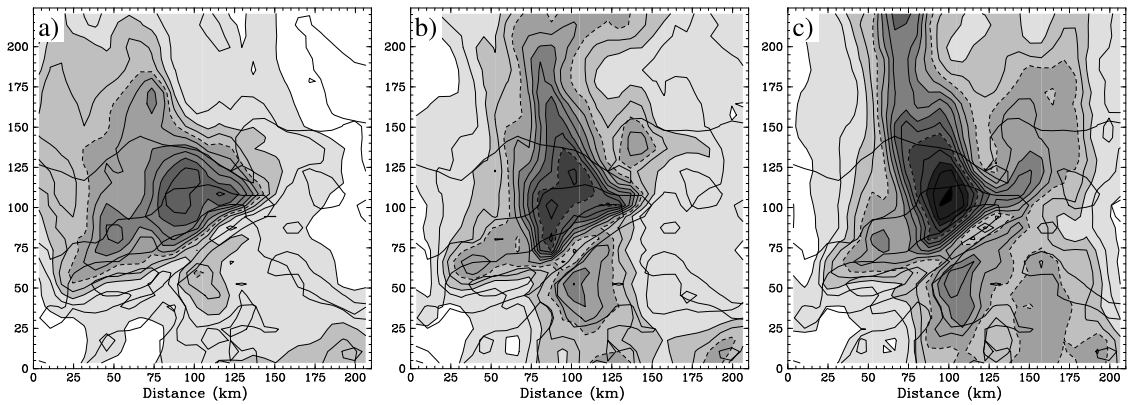

Figure 5: Same as Fig. 3, but for experiments (a) EC-LM-1112, (b) EC-LM-1200, (c) EC-GMI60-LM-1200.

precipitation maximum is still mislocated, leading to a high FAR above 200 mm in the 1200 case. Finally, Fig. 4f confirms that the skill of the EC-GMI60-LM series is not as good as for the EC-LM series.

All six experiments initialized with ECMWF analysis data have been repeated with the prognostic precipitation scheme in the LM (LMpp series). Comparing the verification results summarized in Table 1 with those for the diagnostic scheme indicates that the prognostic scheme significantly decreases the total amount of precipitation. This is mostly related to a bug in the prognostic precipitation scheme of the LM version used for this study, leading to a systematic underestimation of the precipitation reaching the ground. A test with the corrected scheme revealed that about 90% of the domain-averaged difference were related to this bug. However, the spatial distribution of the precipitation remained largely unaffected, so that we decided not to repeat the full suite of sensitivity tests. Table 1 reveals that the pattern correlation between the simulated and observed rainfall fields is generally improved by the prognostic scheme, leading to a substantial decrease of the error measures in the 1200 cases. For the 1112 cases, the increased negative bias tends to balance the improved pattern correlation, so that the error measures do not show up a clear trend. With the corrected precipitation scheme, the error measures would be improved in both cases. The accumulated precipitation fields for the EC-LMpp series (Fig. 6a,b) indicate that the improvement of the pattern correlation is mainly due to a downstream shift of the precipitation maximum over the eastern Erzgebirge, bringing it closer to the observed location. This is also true for the EC-GMI-LMpp experiments (not shown). Correspondingly, Figs. 4h and 4i show that the prognostic scheme reduces the FAR and improves the ETS, particularly for the initialization at 1200. The high peak in the FAR appearing for the EC-LMpp-1200 run is represented by very few data points and thus not quite significant.

Taking the lateral boundary data from GME forecasts initialized with ECMWF analyses has a similar impact as for the experiments with the diagnostic precipitation scheme discussed above. Compared to the simulations driven with ECMWF forecasts, the negative bias increases for the 1112 runs while it decreases for the 1200 runs (Table 1 and Figs. 4g,j). Moreover, the verification results are significantly degraded when the GME forecasts are conducted at 60 km resolution. However, the differences between the EC-LMpp and EC-GMI40-LMpp series are even smaller than for the experiments with the diagnostic scheme (Table 1 and Fig. 4j–l), which is corroborated by a visual inspection of the precipitation fields (not shown). This confirms that the initial data have a much larger impact on the forecast skill than the forecast model used for creating the lateral boundary conditions, provided that the spatial resolution of the outer (global) is not too low.

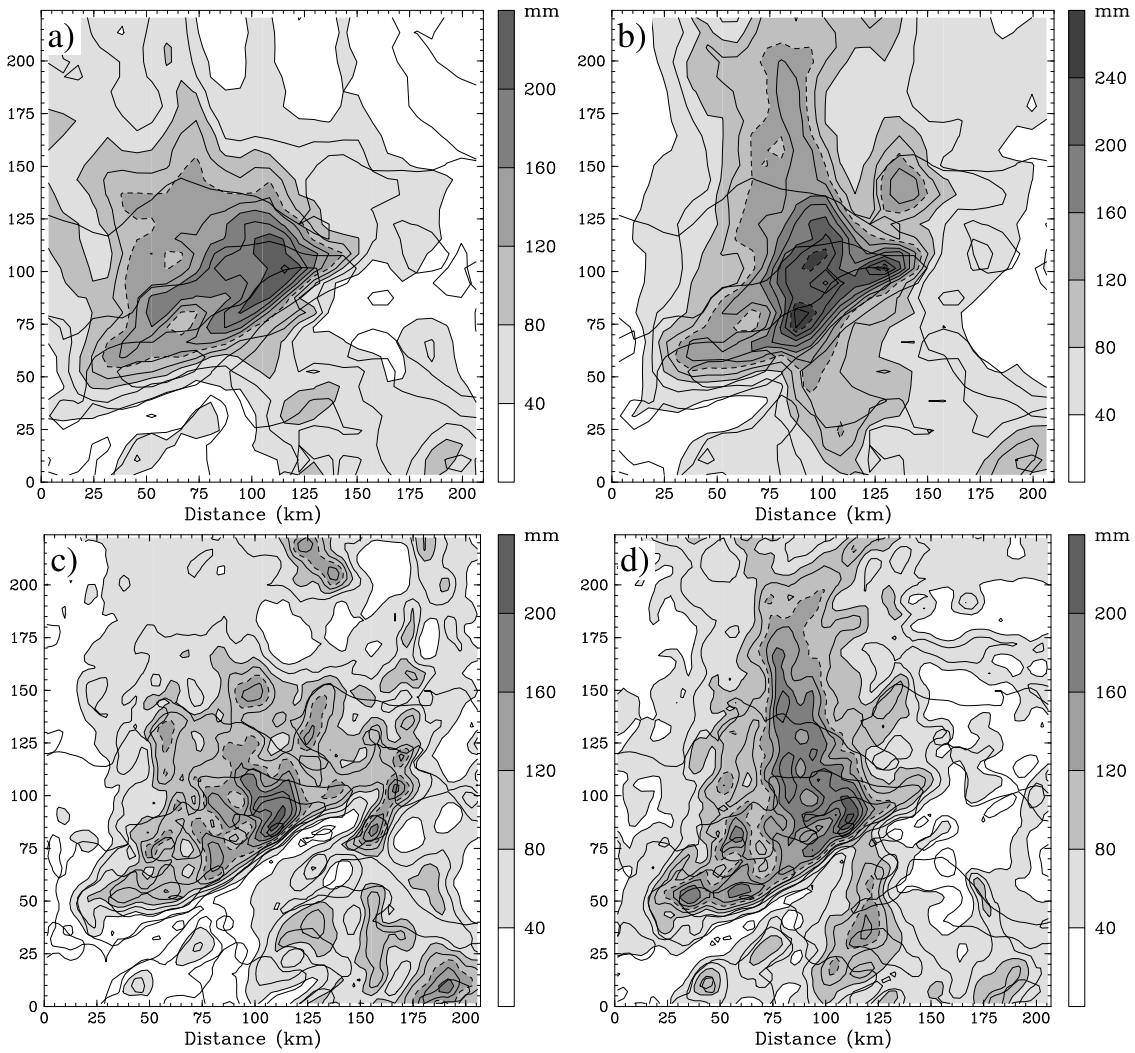

Figure 6: Same as Fig. 3, but for experiments (a) EC-LMpp-1112, (b) EC-LMpp-1200, (c) EC-LMKpp-1112, (d) EC-LMKpp-1200. In (c) and (d), bold lines indicate the LMK topography.

Finally, a look at the results obtained with the LMK configuration (2.8 km mesh size, Fig. 6c,d) reveals that the increased resolution creates much smaller-scale structures in the precipitation fields. This is partly due to a better resolution of the topography and partly due to the fact that the convection scheme is switched off in the LMK experiments. However, a comparison with the corresponding LM runs (Fig. 6a,b) shows that the total amount of precipitation, including the precipitation maxima, is less for the LMK than for the LM. This implies an increased negative bias (Table 1 and Fig. 4g). Moreover, Table 1 and Fig. 4i indicate that the forecast skill of our preliminary LMK version is not as good as that of the LM. A larger number of LMK experiments should be conducted when the development of the model code is completed. In particular, recent tests performed at DWD revealed that a shallow convection parameterization is still necessary at a mesh size of 2.8 km in order to improve the triggering of resolved deep convection.

5. Conclusions

Our sensitivity tests for the Elbe flood case indicate that the limited accuracy of the initial data was the most important reason for the poor quality of the operational forecasts. At least

in the present case, the sophisticated 4D-VAR data assimilation performed at ECMWF leads to a substantially better forecast accuracy than the optimal interpolation scheme currently used in the GME. This is in accordance with the notion that forecasts of extreme weather events are particularly sensitive to the accuracy of the initial data (e.g. Wergen and Buchhold, 2002). Thus, the 3D-VAR scheme currently under development for the GME can be regarded as an important step for improving the forecast skill. On the other hand, our experiments in which a GME forecast initialized with ECMWF analysis data was used to provide the lateral boundary conditions for the LM indicate that the global model itself is of comparatively minor importance. It is mainly its horizontal resolution that plays a role. A mesh size of 40 km, as currently used both in the GME and the ECMWF model, yields significantly better results than a mesh size of 60 km (operational in the GME prior to October 2004). In addition, a comparison of the cloud microphysics schemes available in the LM shows that accounting for the downstream advection of precipitation particles is important to get the spatial structure of the precipitation right. The impact is particularly evident over the Erzgebirge, where the rainfall maximum is shifted from the windward slope toward the crest line.

To relate our present results to the MM5 simulations reported in Z04, it has to be mentioned that the MM5 simulations were driven with ECMWF analysis data rather than forecast data and that the MM5 was operated in a multiple-nested configuration with 2–4 domains and a finest resolution of 9 km, 3 km and 1 km, respectively. Thus, the results are not strictly comparable with the LM forecasts. Nevertheless, the verification results of EC-LMpp-1112 are very close to the two-domain MM5 run with a finest resolution of 9 km, and EC-LMpp-1200 performs even better than a corresponding MM5 simulation initialized at 1200 (not reported in Z04). However, the dependence of the model skill on the horizontal resolution is opposite. While the MM5 verification results steadily improve with increasing model resolution (see Z04), the 2.8-km resolution LMK performs not as well as the 7-km LM (implying that it is also inferior to the MM5 at 3 km resolution). The most likely explanation for this puzzling behaviour lies in the different characteristics of the convection parameterizations. The Kain-Fritsch scheme used in the 9-km MM5 domain (Kain and Fritsch, 1993) accounts for less than 3% of the total precipitation in the core precipitation area (Erzgebirge), whereas the Tiedtke scheme of the LM accounts for 20–25% of the total precipitation. In the MM5, the domain-average precipitation then increases with increasing horizontal resolution because resolved embedded convection enhances the precipitation efficiency of the microphysical scheme. This reduces the negative bias and improves the skill scores. In the LM, however, the convection scheme appears to overcompensate the resolution-dependence of explicit precipitation, leading to an opposite behaviour of total precipitation and skill scores. Another contribution probably arises from the lack of an appropriate shallow convection scheme in the LMK, which was not yet available for our tests.

Acknowledgements

The DWD and the CHMI (Czech Hydrometeorological Institute) are acknowledged for providing the raingauge data needed for validating the model results.

References

van Bebber, J. W., 1891: Die Zugstraßen der barometrischen Minima. (The tracks of the barometric minima.) *Meteor. Zeitschr.*, 8, 361–366.

DWD, 2002: Starkniederschläge in Sachsen im August 2002. (Heavy precipitation in Saxony in August 2002.) Internal report, Deutscher Wetterdienst, Offenbach, October 2002, 61 pp.

Hartjenstein, G., G. Zängl, G. Doms, H. Frank, and U. Schättler, 2005: Numerical simulations of the Elbe flood case: Sensitivity to initial and boundary data. Proc. Intern. Conf. on Alpine Meteorology, Zadar, Croatia, *Croat. Meteorol. Journal,* 70, 361–364.

Kain, J. S. and J. M. Fritsch, 1993: Convective parameterization for mesoscale models: The Kain-Fritsch scheme. *The representation of cumulus convection in numerical models*, K. A. Emanuel and D. J. Raymond, Eds., Amer. Meteor. Soc., 246 pp.

Steppeler, J., G. Doms, U. Schättler, H.-W. Bitzer, A. Gassmann, U. Damrath, and G. Gregoric, 2003: Meso-gamma scale forecasts using the nonhydrostatic model LM. *Meteorol. Atmos. Phys.,* 82, 75–96.

Tiedtke, M, 1989: A comprehensive mass flux scheme for cumulus parameterization in large-scale models. *Mon. Wea. Rev.,* 117, 1779–1799.

Tustison, B., D. Harris, and E. Foufoula-Georgiou, 2001: Scale issues in verification of precipitation forecasts. *J. Geophys. Res.,* 106, 11775–11784.

Ulbrich, U., T. Brücher, G. C. Leckebusch, A. Krüger, and J. G. Pinto, 2003: The central European floods of August 2002: Part II – Synoptic causes and considerations with respect to climate change. *Weather*, 58 (11), 434–441.

Wergen, W., and M. Buchhold, 2002: Datenassimilation für das Globalmodell GME. (Data assimilation for the global model GME.) *Promet,* 27, 150–155.

Zängl, G., 2004: Numerical simulations of the 12–13 August 2002 flooding event in eastern Germany. *Quart. J. Roy. Met. Soc.,* 130, 1921–1940.